Strain Control of Domain Structures in Ferroelectric Thin Films: Applications of Phase-Field Method

49

Jian-Jun Wang and Long-Qing Chen

Contents

Abstract

Ferroelectric thin films have potential applications in many devices such as memories, microwaves, transduction sensors, actuators, photovoltaics, etc. The mesoscale domain structures and thus properties of ferroelectric thin films depend crucially on the amount of strain imposed upon by the underlying substrates. Phase-field method has been extensively applied to understanding the underlying physics of the experimentally observed domain structures and predicting their responses to external electrical, mechanical, thermal, and chemical stimuli. In this chapter, the fundamentals of the thin-film phase-field method and its applications in predicting the effects of strains on the phase transitions,

J.-J. Wang · L.-Q. Chen (✉)
Department of Materials Science and Engineering, The Pennsylvania State University, Pennsylvania, PA, USA
e-mail: wjj8384@gmail.com; lqc3@psu.edu

W. Andreoni, S. Yip (eds.), *Handbook of Materials Modeling*,
https://doi.org/10.1007/978-3-319-44680-6_60

domain structures, and the domain switching are reviewed. The prospect of using phase-field method in microstructure design and property optimization for ferroelectric thin films is discussed.

1 Introduction

The advances in film-growth methods including the pulsed laser deposition (PLD) (Ramesh et al. 1990; Hubler 1992; Frey et al. 1994; Koster et al. 1999) and molecular beam epitaxy (MBE) (Chao and Arthur 1975; Spah et al. 1988; Schlom et al. 1988; Kwo et al. 1988; Eckstein and Bozovic 1995; Theis et al. 1998) have allowed the growth of high-quality epitaxial ferroelectric thin films. An in-plane biaxial strain is typically generated and imposed on the film via the epitaxial lattice mismatch. Compared with the ferroelectric bulk counterparts which would normally fracture under moderate strains such as $\sim\pm0.1\%$, epitaxial thin films can withstand much larger in-plane biaxial strains up to $\sim\pm3\%$ (Schlom et al. 2007, 2008, 2014; Martin and Rappe 2017). Owing to the strong coupling between the polarization and the lattice degrees of freedom in ferroelectrics, novel phases, physics, and properties may emerge in heavily strained thin films. For example, a stress-free $SrTiO_3$ crystal is paraelectric down to 0 K. However, when a (001)-oriented $SrTiO_3$ was epitaxially grown on a (110)-oriented $DyScO_3$ substrate which can impose a tensile biaxial strain of $\sim0.8\%$ on $SrTiO_3$ film, a room-temperature ferroelectricity was observed in the $SrTiO_3$ thin film (Haeni et al. 2004). The similar effect was observed in strained $BaTiO_3$ thin films which show enhanced room-temperature remnant polarization and ferroelectricity at temperatures much higher than the bulk Curie point (Choi et al. 2004). While a stress-free $BiFeO_3$ bulk crystal has a stable rhombohedral symmetry below the Curie temperature of 830 °C (Catalan and Scott 2009), a $BiFeO_3$ thin film on a $LaAlO_3$ substrate is subjected to a huge compressive strain ($\sim-4.5\%$) and was shown to exhibit a highly distorted tetragonal symmetry. As thickness of a $BiFeO_3$ film increases, it gradually loses the coherency strains, leading to the formation of a rhombohedral-tetragonal alternating "stripe-like" mixed-phase structure (Zeches et al. 2009; Li et al. 2015).

The thermodynamic analysis was normally performed to understand the strain effect on the phase transition of ferroelectric thin films (Pertsev et al. 1998; Roytburd 1998; Sheng et al. 2008; Shirokov et al. 2009; Qiu et al. 2010). It starts from the Landau phenomenological theory of a ferroelectric bulk crystal, wherein the Gibbs energy density is used to describe the total free energy of the bulk system with temperature, electric field, and the stress as independent variables. For studying the effect of strain on transition temperatures, it is actually more convenient to use strain rather than stress as the independent variable. Therefore, a Legendre transformation can be performed to obtain the Helmholtz free energy density, in which strain is the independent variable in the mechanical energy term. The stress components can be solved from the combination of thermodynamic property equations (first-order derivatives of the Gibbs free energy) and the mechanical boundary conditions of the epitaxial thin film. More specifically, the first-order derivative of the Gibbs free

energy with respect to a stress component is equal to the corresponding negative strain component. The in-plane strain components of the thin film are fixed by the film/substrate lattice mismatch due to interfacial coherency, and the out-of-plane stress components of the thin film are zero due to the traction-free film surface. Eventually, the equilibrium state and the thermodynamic properties of the thin film can be established by minimizing the total thermodynamic potential of the thin film with respect to the thermodynamic variables.

The thermodynamic analysis has been extensively employed to predict the strain-temperature phase diagrams of various ferroelectric thin films including $PbTiO_3$ (Pertsev et al. 1998; Zembilgotov et al. 2005), $PbZr_{1-x}Ti_xO_3$ (Pertsev et al. 2003; Li et al. 2003a; Qiu et al. 2010), $BaTiO_3$ (Emelyanov et al. 2002; Shirokov et al. 2007; Sheng et al. 2008), $BiFeO_3$ (Zhang et al. 2007; Ma et al. 2008; Karpinsky et al. 2017), etc. One advantage of the thermodynamic analysis is the easy implementation of the thermodynamic potential into MATHEMATICA or MATLAB programs. Using the "minimization function" built in the software, the thermodynamic potential can be conveniently minimized to obtain the equilibrium state and the polarization-related properties such as the polarization, spontaneous strain, dielectric permittivity, and piezoelectric coefficients. However, when considering polydomain structures, the thermodynamic analysis becomes much more complicated (Kouhar et al. 2001; Bratkovsky and Levanyuk 2002; Xu et al. 2015). Moreover, there is no direct access or even impossible to get the kinetic behavior of the polarization and properties on the domain walls through the thermodynamic analysis. In order to achieve this, the interfacial energy or domain wall energy and the time-evolving behavior of the polarization need to be considered.

2 Phase–Field Method

Phase-field method combines the material thermodynamics and kinetics. It has become an important tool for studying microstructure evolution (Chen 2002; Boettinger et al. 2002; Gránásy et al. 2006; Chen 2008; Steinbach 2009). The phase-field method for ferroelectric epitaxial thin films was firstly developed by Li et al., and it has been employed to study the strain-temperature phase diagrams, domain structures, domain switching, and other domain-related properties for various ferroelectric thin films (Li et al. 2001, 2002a, 2002b, and 2003b, 2006; Li and Chen 2006; Zhang et al. 2008; Kontsos and Landis 2010; Winchester et al. 2011; Britson et al. 2014; Hong et al. 2014; Chen et al. 2014; Wang et al. 2016). In the phase-field method of ferroelectric thin films, the polarization vector is selected as the order parameter. The spatial distribution of the polarization represents the domain structures of a thin film. The evolution of polarization can be described by the time-dependent Landau-Ginzburg (TDGL) equations, i.e.:

$$\frac{\partial \mathbf{P}(\mathbf{x}, t)}{\partial t} = -L \frac{\delta F}{\delta \mathbf{P}(\mathbf{x}, t)}, \tag{1}$$

where $\mathbf{P}$, $\mathbf{x}$, t, F, and L represent the polarization vector, spatial coordinate, time, the total free energy of the thin-film system, and the kinetic coefficient that is related to the domain wall mobility, respectively.

In the phase-field method of ferroelectric thin films (Li et al. 2001; Chen 2008), only polarization-related energy contributions are considered in the total free energy, which normally includes the Landau energy (bulk chemical energy), elastic energy, electric energy, and gradient energy, i.e.:

$$F = \iiint_V \left[f_{\text{bulk}}\left(\mathbf{P}, T\right) + f_{\text{grad}}\left(\nabla \mathbf{P}\right) + f_{\text{electric}}\left(\mathbf{P}, \mathbf{E}\right) + f_{\text{elastic}}\left(\mathbf{P}, \boldsymbol{\varepsilon}\right) \right] dV, \tag{2}$$

where $f_{\text{bulk}}, f_{\text{grad}}, f_{\text{electric}}, f_{\text{elastic}}$, $\boldsymbol{\varepsilon}$, $\mathbf{E}$, and $\nabla \mathbf{P}$ represent the bulk, gradient, electric, elastic energy densities, strain tensor, electric field vector, and polarization gradient, respectively. The bulk energy density can be expressed by a Landau polynomial as function of polarization, i.e.:

$$\begin{aligned} f_{\text{bulk}} = {} & \alpha_1 \left(P_1^2 + P_2^2 + P_3^2\right) + \alpha_{11} \left(P_1^4 + P_2^4 + P_3^4\right) \\ & + \alpha_{12} \left(P_1^2 P_2^2 + P_1^2 P_3^2 + P_2^2 P_3^2\right) + \alpha_{111} \left(P_1^6 + P_2^6 + P_3^6\right) \\ & + \alpha_{112} \left[P_1^4 \left(P_2^2 + P_3^2\right) + P_2^4 \left(P_1^2 + P_3^2\right) + P_3^4 \left(P_1^2 + P_2^2\right)\right] \\ & + \alpha_{123} P_1^2 P_2^2 P_3^2 + \alpha_{1111} \left(P_1^8 + P_2^8 + P_3^8\right) \\ & + \alpha_{1122} \left(P_1^4 P_2^4 + P_1^4 P_3^4 + P_2^4 P_3^4\right) \\ & + \alpha_{1112} \left[P_1^6 \left(P_2^2 + P_3^2\right) + P_2^6 \left(P_1^2 + P_3^2\right) + P_3^6 \left(P_1^2 + P_2^2\right)\right] \\ & + \alpha_{1123} \left(P_1^4 P_2^2 P_3^2 + P_1^2 P_2^4 P_3^2 + P_1^2 P_2^2 P_3^4\right), \end{aligned} \tag{3}$$

where α_i, α_{ij}, α_{ijk}, and α_{ijkl} are called Landau coefficients relating to the different-order dielectric stiffness. They can be fitted to the bulk properties at zero stress (Haun et al. 1989a; 1989b; 1989c; Li et al. 2005; Wang et al. 2007; Liang et al. 2009; Pohlmann et al. 2017).

The gradient energy density is defined as

$$f_{\text{grad}} = \frac{1}{2} \gamma_{ijkl} P_{i,j} P_{k,l}, \tag{4}$$

where γ_{ijkl} are the components of the gradient energy coefficient tensor and $P_{i,j}$=$\partial P_i / \partial x_j$.

The electric energy density is given by:

$$f_{\text{electric}} = -P_i\left(\mathbf{x}\right) E_i\left(\mathbf{x}\right) - \frac{1}{2} \varepsilon_0 \kappa_{ij}^{\text{b}} E_i\left(\mathbf{x}\right) E_j\left(\mathbf{x}\right), \tag{5}$$

where κ_{ij}^{b} are components of the background dielectric constant tensor (Rupprecht and Bell 1964; Tagantsev 2008). The electric field distribution can be solved from

the electrostatic equilibrium equation, which can be dramatically affected by the electric boundary condition. For example, under open-circuit boundary conditions, if the bound charges at the film surfaces are not compensated, a depolarization field will be generated and may significantly suppress the polarization. This effect will be dominant when the thickness of the thin film is down to several unit cells, leading to the disappearance of the ferroelectricity, which is also called the size effect of the ferroelectric thin films (Scott 1988, 1991; Junquera and Ghosez 2003).

The elastic energy density can be calculated according to the Hooke's law:

$$f_{\text{elastic}} = \frac{1}{2} c_{ijkl} e_{ij}(\mathbf{x})\, e_{kl}(\mathbf{x}) = \frac{1}{2} c_{ijkl} \left[\varepsilon_{ij}(\mathbf{x}) - \varepsilon^0_{ij}(\mathbf{x})\right] \left[\varepsilon_{kl}(\mathbf{x}) - \varepsilon^0_{kl}(\mathbf{x})\right], \tag{6}$$

where c_{ijkl} are components of the elastic stiffness tensor and $e_{ij}(\mathbf{x})$, $\varepsilon_{ij}(\mathbf{x})$, and $\varepsilon^0_{ij}(\mathbf{x})$ are components of the elastic strain tensor, total strain tensor, and eigenstrain tensor, respectively. The eigenstrain tensor $\varepsilon^0_{ij}(\mathbf{x})$, or the stress-free strain tensor, arises from the coupling between the polarization and the lattice degrees of freedom in ferroelectrics. This coupling is also named the electrostrictive effect (Cross et al. 1980; Cross 1996; Sundar and Newnham 1992). It is a universal effect in insulators, and in ferroelectrics the quadratic coupling can be especially strong. The strength of the quadratic coupling between polarization and the lattice degrees of freedom is described by the electrostrictive coefficient Q_{ijkl}, which is a fourth-order tensor. Its values can be obtained by experimental measurements (Yamada 1972) or first-principle calculations (Wang et al. 2010). The eigenstrain $\varepsilon^0_{ij}(\mathbf{x})$ can be calculated from $\varepsilon^0_{ij}(\mathbf{x}) = Q_{ijkl} P_k(\mathbf{x}) P_l(\mathbf{x})$. The total strain $\varepsilon_{ij}(\mathbf{x})$ can be solved from the mechanical equilibrium equation using Khachaturyan's microelasticity theory (Khachaturyan 1983), in combination with the thin-film mechanical boundary conditions (Li et al. 2002).

In the phase-field model of ferroelectric thin film, materials parameters needed include the Landau coefficients, gradient energy coefficients, background dielectric constant tensor, elastic compliance tensor, and electrostrictive coefficient tensor. With these materials parameters available, the domain structures under different temperatures and in-plane biaxial strain conditions can be obtained starting from a random distribution of polarization or from an existing domain structure.

3 Phase Transitions and Domain Structures

In the phase-field simulation of ferroelectric thin films, the equilibrium domain structures can be predicted by quenching an annealed paraelectric state with a fixed substrate constraint to lower temperatures. The main advantage of the phase-field method is the fact that one does not have to make a priori assumptions on the possible ferroelectric phases and domain structures that might appear under a given temperature and an epitaxial strain.

3.1 Misfit Strain–Temperature Phase Diagrams

The phase-field method has been employed to calculate the strain-temperature phase diagrams for several ferroelectric thin-film oxides such as $PbTiO_3$ (Li et al. 2001), $BaTiO_3$ (Choi et al. 2004), $SrTiO_3$ (Haeni et al. 2004), and $PbZr_{1-x}Ti_xO_3$ (Choudhury et al. 2005) (Fig. 1a–d). A common feature of these phase diagrams is the enhanced Curie temperature by the epitaxial strain. This effect can be dramatic as the Curie temperature can be increased by several hundred degrees by only 1% compressive or tensile strain. This effect originates from the strong coupling between the polarization and the lattice degrees of freedom. Another common feature among these phase diagrams is the existence of transition regions along the ferroelectric/paraelectric phase boundaries. For the stress-free bulk ferroelectrics including $PbTiO_3$, $BaTiO_3$, $SrTiO_3$, and $PbZr_{1-x}Ti_xO_3$, the phase transition is normally first-order at which the polarization changes sharply at the transition temperature. However, under thin-film mechanical boundary conditions with con-

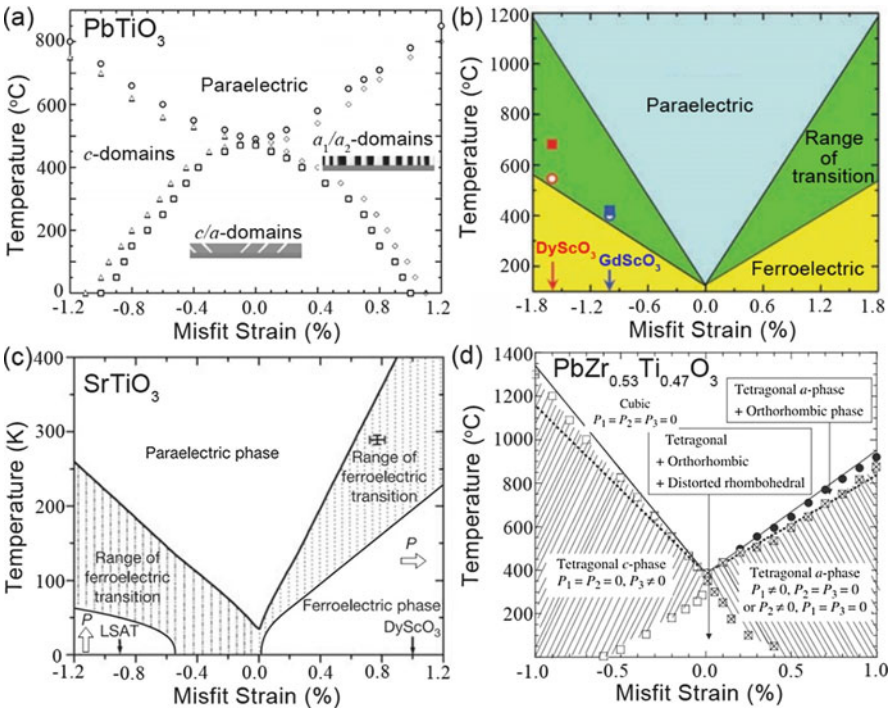

Fig. 1 Misfit strain-temperature phase diagrams of (**a**) $PbTiO_3$ (adapted from Li et al. 2001), (**b**) $BaTiO_3$ (adapted from Choi et al. 2004), (**c**) $SrTiO_3$ (adapted from Haeni et al. 2004), and (**d**) $PbZr_{0.53}Ti_{0.47}O_3$ (adapted from Choudhury et al. 2005) thin films predicted using the phase-field method. (Copyright 2001, American Institute of Physics, Copyright 2004 American Association for the Advancement of Science, Copyright 2004, Springer Nature, Copyright 2001, American Institute of Physics)

straint strains in-plane and stress-free out-of-plane, the paraelectric to ferroelectric phase transition may become second-order (Pertsev et al. 1999). This is caused by the renormalization of the fourth-order Landau coefficients due to the coupling between the polarization and the strain. On the strain-temperature phase diagram of $PbTiO_3$ thin film (Fig. 1a), there is a large region wherein the in-plane *a* domain and out-of-plane *c* domain can coexist, which has been verified by numerous experimental observations (Seifert et al. 1995; Kiguchi et al. 2011; Tang et al. 2014). For $PbZr_{0.53}Ti_{0.47}O_3$ thin film shown in Fig. 1d, there are also some mixed-phase regions. For example, under moderate strains and low temperatures, the tetragonal phase, orthorhombic phase, and distorted rhombohedral phase may coexist. These mixed-phase regions are normally not predicted from thermodynamic analysis without considering the multi-domain structures.

3.2 Domain Structures in Single–Layered Thin Films

A common feature of ferroelectric materials is the formation of domain structures when the material is cooled down from a paraelectric phase to a ferroelectric phase. A ferroelectric domain is defined by a region with uniform electrical polarization. The domain size may range from several nanometers to hundreds of nanometers depending on many factors such as the film thickness, the epitaxial strain, and the electric boundary conditions. The type of domain structures is determined by the total free energy, which can be altered by external stimuli including the mechanical, electric, thermal, and chemical stimuli. One advantage of phase-field modeling of the domain structures in ferroelectric thin films is the theoretically feasible incorporation of arbitrary boundary conditions, although only some of the possible boundary conditions can be realized in experimental configurations.

By incorporating materials parameters and incorporating boundary conditions of the experimental thin films into the phase-field model, the equilibrium domain structures can be obtained and compared with available experimental observations. For example, Fig. 2a shows the *a*/*c* domain structures predicted in a (001)-oriented $PbTiO_3$ thin film under a moderate compressive strain, while Fig. 2b gives the domain structures observed in a $PbTiO_3$ thin film epitaxially grown on a (001)-oriented $SrTiO_3$ substrate which can impose a compressive strain on the $PbTiO_3$ thin film. The *a* domain represents the domains with the polarization along either the x_1 or x_2 axis of the pseudocubic lattice, and the *c* domain represents the domains with the polarization along the x_3 axis of the pseudocubic lattice. The predicted domain structures (Li et al. 2002) show amazing similarity to the domain structures observed (Seifert et al. 1995) using the transmission electron microscopy (TEM). The formation of the *a*/*c* domain structures can be understood from the competition between the elastic energy, the electrostatic energy, and the gradient energy. For the moderately compressed thin films under short-circuit electric boundary conditions, a single *c* domain can minimize the electrostatic energy and the gradient energy. In this case however the macroscopic deformation along the out-of-plane direction will be maximized, leading to a high elastic energy. Therefore, some *a* domains

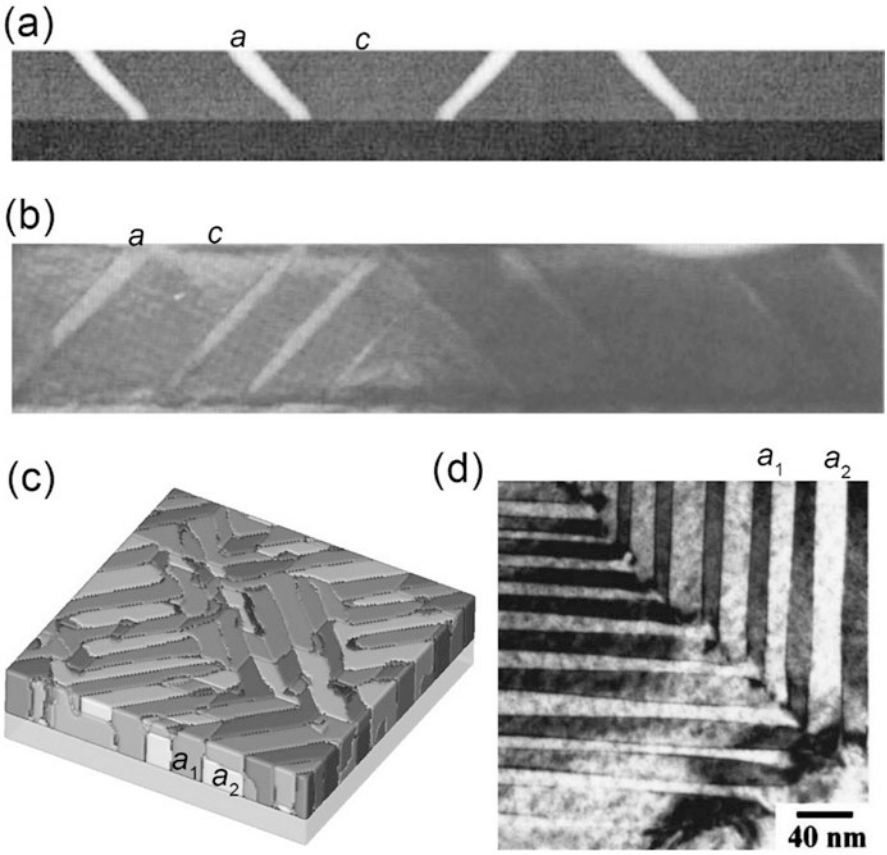

Fig. 2 (**a**) Predicted *a*/*c* domain structures in a (001)-oriented $PbTiO_3$ thin film under moderate compressive strains (adapted from Li et al. 2002), compared with (**b**) the experimental observation in a $PbTiO_3$ thin film epitaxially grown on a (001)-oriented $SrTiO_3$ substrate (adapted from Seifert et al. 1995). (**c**) Predicted a_1/a_2 twinning domain structures in a $PbZr_{0.2}Ti_{0.8}O_3$ thin film under equally biaxial tensile strains (adapted from Wang et al. 2016), compared with (**d**) the experimental observation in a $PbTiO_3$ thin film epitaxially grown on a (001)-oriented $KTaO_3$ substrate. (Adapted from Lee et al. 2001. Copyright 2002, 2016, Elsevier, Copyright 2001, American Institute of Physics)

are generated to decrease the macroscopic deformation and the elastic energy but comprise to slightly increase the electrostatic energy and the gradient energy.

3.3 Domain Structures in Bilayer Thin Films

The phase-field method was also employed by Artemev et al. to study the domain structures in ferroelectric bilayer thin films (Artemev et al. 2008). They found that a poled state can be achieved by a low electric field in the bilayer film with one layer

in a single-domain state and the other layer in a polydomain state. In contrast to the bilayer film with both layers in single-domain states, the presence of a polydomain layer in the bilayer film is responsible for a higher dielectric constant and lower coercive field. The increase in the applied electric field can lead to a transition to single-domain states in both layers of the bilayer film, and the critical field depends on the thermodynamic potentials of the two layers (Artemev et al. 2008). Using the thin-film phase-field method, Xue et al. investigated the effect of interfacial coherency between the two layers in a $Pb(Zr_{0.3}Ti_{0.7})O_3/Pb(Zr_{0.7}Ti_{0.3})O_3$ bilayer thin films on the domain structures (Xue et al. 2013). If the lattice parameters of the two layers end up with the same average lattice parameter, the two layers can be regarded as coherent. For example, the cubic lattice parameters for $Pb(Zr_{0.3}Ti_{0.7})O_3$ and $Pb(Zr_{0.7}Ti_{0.3})O_3$ are 4.0185 Å and 4.1032 Å, respectively, giving rise to an average lattice parameter of 4.0609 Å when the two layers have the same thickness. With a coherent interface, the strained bilayer film has a lattice parameter of 4.0609 Å. Consequently, the $Pb(Zr_{0.3}Ti_{0.7})O_3$ layer tolerates a tensile strain of $(4.0609-4.0185)/4.0185 = 1.05\%$, and the $Pb(Zr_{0.7}Ti_{0.3})O_3$ layer tolerates a compressive strain of $(4.0609-4.1032)/4.1032=-1.03\%$. For a totally incoherent bilayer film, each layer can be regarded to have similar lattice parameters to their bulk counterparts, unless the clamping effect from the substrate is considered.

The interfacial coherency has significant effects on the domain structures in each layer (Fig. 3a and b). For $Pb(Zr_{0.3}Ti_{0.7})O_3/Pb(Zr_{0.7}Ti_{0.3})O_3$ bilayer thin films with coherent interface, tetragonal a_1/a_2 twinning domain structures (all in-plane polarizations) are predicted in the $Pb(Zr_{0.3}Ti_{0.7})O_3$ layer (Fig. 3a), while in its single-layer thin film, the domain structures are tetragonal *a*/*c* types (Fig. 3c, mixed in-plane and out-of-plane polarizations). The $Pb(Zr_{0.7}Ti_{0.3})O_3$ layer in the bilayer film shows tetragonal *c* domains (all out-of-plane polarizations), compared with rhombohedral domains in its single-layer thin-film counterpart (Fig. 3d). For the bilayer film with incoherent interface, the domain structures in each layer are similar to their single-layer thin-film counterparts, i.e., *a*/*c* domains in $Pb(Zr_{0.3}Ti_{0.7})O_3$ layer and rhombohedral domains in $Pb(Zr_{0.7}Ti_{0.3})O_3$ layer (Fig. 3b). The interfacial coherency effects on the domain morphologies can be understood from the strain configuration in the bilayer film. In $Pb(Zr_{0.3}Ti_{0.7})O_3$ layer, the tensile strain 1.05% tends to align all polarizations in-plane, leading to the formation of a_1/a_2 twinning domain structures under the synergistic effect from the bulk chemical energy and elastic energy. In $Pb(Zr_{0.7}Ti_{0.3})O_3$ layer, the compressive strain −1.03% tends to switch all polarizations out-of-plane, leading to the formation of *c* domains (Xue et al. 2013; Liu et al. 2016).

3.4 Strain Phase Separation

The thin-film phase-field model was also used to understand the formation of mixed phases and domains in strained thin films from the perspective of strain phase separation. In a constrained system, domains or phases can form and coexist with each other to minimize the overall elastic energy, given that each domain or phase

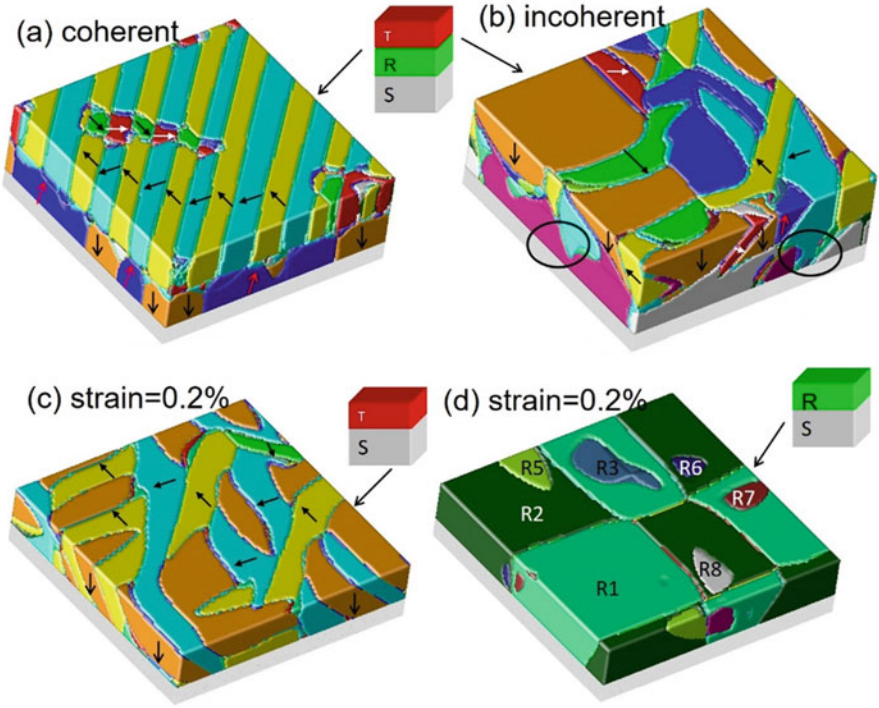

Fig. 3 Effects of interfacial coherency on the domain structures in a $Pb(Zr_{0.3}Ti_{0.7})O_3/Pb(Zr_{0.7}Ti_{0.3})O_3$ bilayer thin film (Xue et al. 2013). Domain structures of the bilayer film when the interface between the two layers is (**a**) coherent and (**b**) incoherent, compared with the domain structures in single-layer (**c**) $Pb(Zr_{0.3}Ti_{0.7})O_3$ thin film and (**d**) $Pb(Zr_{0.7}Ti_{0.3})O_3$ thin film under a moderate strain of 0.2% due to thermal expansion. (Copyright 2013, Elsevier)

has different local strains. This phenomenon is similar to the phase decomposition process from a chemically homogeneous phase to a two-phase mixture wherein each phase has a different chemical composition. The volume fraction of each phase with a specific composition can be obtained from the lever rule. This idea was used to understand the observed rhombohedral-tetragonal mixed phases in severely compressed $BiFeO_3$ thin films (Xue et al. 2016, 2017). $BiFeO_3$ has a pseudocubic lattice parameter of ~4.0 Å. When it is epitaxially grown on a $LaAlO_3$ substrate with a lattice parameter of ~3.79 Å, a large compressive strain up to ~−5.25% will be imposed on the thin film, leading to a transition from the rhombohedral phase to a tetragonal-like monoclinic phase in $BiFeO_3$ thin film (Zeches et al. 2009; Li et al. 2015; Zhang et al. 2012). With the film thickness increasing to be larger than 100 nm, the large epitaxial strain is partially relaxed, and the rhombohedral phase emerges, forming a tetragonal-like/rhombohedral mixed domain structure (Fig. 4a

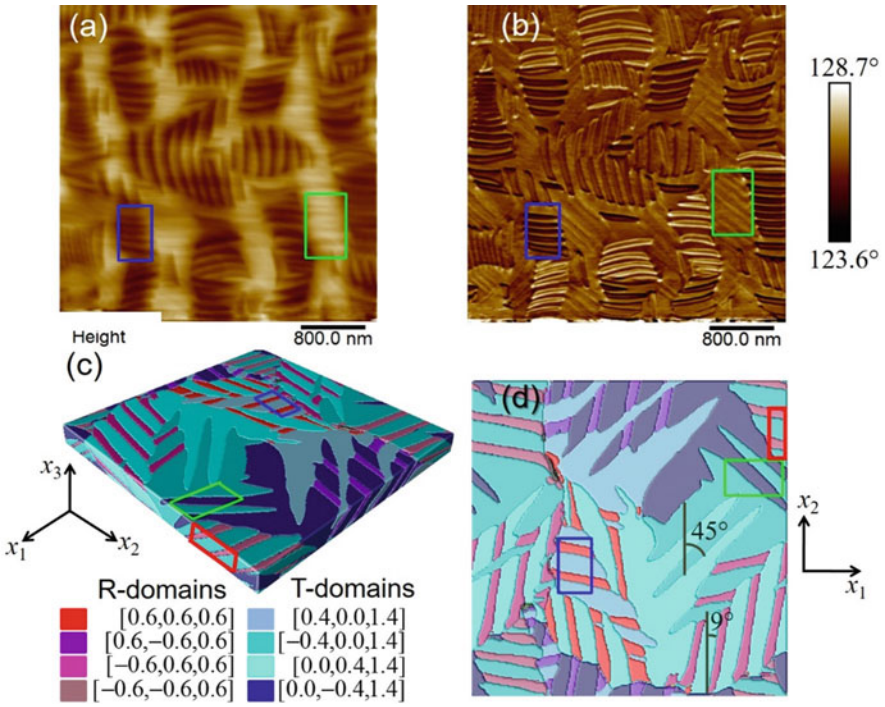

Fig. 4 Experimentally observed (**a**) topography and (**b**) the corresponding in-plane piezoresponse force microscopy result of a mixed-phase $BiFeO_3$ thin film grown on $LaAlO_3$ substrate, compared with the simulated (**a**) three-dimensional domain structures and (**b**) in-plane domain morphology from thin-film phase-field method. (Adapted from Xue et al. 2016. Copyright 2016, American Physics Society)

and b). The phase-field model was employed to predict domain structures (Fig. 4c and d) which agree well with the experimental observations and give insights to the underlying physics. With the relaxation of the mismatch strain, the overall strain will be smaller than the critical strain, under which the transition from rhombohedral phase to tetragonal-like phase occurs. Therefore, the phase separation happens to decrease the total elastic energy, analogous to the chemical decomposition process (Xue et al. 2016, 2017).

3.5 Understanding the Polarization Switching in Ferroelectric Thin Films

One advantage of the phase-field method over the thermodynamic analysis is the capability of studying the polarization switching behavior in ferroelectric thin films. The polarization switching driven by externally applied electric fields was simulated

by Li et al. for epitaxial $BaTiO_3$ thin films (Li et al. 2008). They found that the coercive field and saturated polarization in the hysteresis loop strongly depend on the type and density of the interfacial dislocation. For example, the coercive field can be decreased by increasing the density of interfacial misfit dislocations on a (100) slip plane with a Burger vector along [−100] direction. With an optimal combination of different misfit dislocations, the remnant polarization can be greatly enhanced and the coercive field can be greatly reduced. The polarization versus electric field hysteresis loops can be distorted to be asymmetric by threading dislocations. Wu et al. investigated the effects of background dielectric constant and interfacial coherency on the hysteresis loops in $BaTiO_3/SrTiO_3$ bilayer films (Wu et al. 2012, 2015). It was found that the hysteresis loops can be constricted when the background dielectric constant is decreased. The decrease in the background dielectric constant has a similar effect to the decrease in the space charge density. The phase-field simulation predicted the domain structure evolution during the switching process in the ferroelectric/paraelectric bilayer film, revealing a dipole-dipole interaction similar to the exchange-spring interaction in magnetic multilayer systems (Wu et al. 2012). The interfacial coherency also has a remarkable impact on the polarization switching behavior. In the bilayer film with fully coherent interfaces, the hysteresis loops are square-like, exhibiting a large coercive field and a large remnant polarization. For the bilayer films with partially relaxed heterointerfaces, the remnant polarization is relatively high but the coercive field is dramatically reduced. For the bilayer film with fully relaxed heterointerfaces, the hysteresis loops are very slim, showing both small remnant polarization and coercive field.

The polarization switching is normally achieved by the externally applied electric field. However, it can also be achieved by a mechanical loading via the flexoelectric effects in epitaxial thin films. The flexoelectric effect is defined as the coupling between the polarization and the strain gradient. This effect is much stronger in ferroelectric thin films than in their bulk counterparts. It has been implemented into the thin-film phase-field model by several research groups (Chen et al. 2014; Ahluwalia et al. 2014; Gu et al. 2014; Chen et al. 2015). In these works, the flexoelectric effects on the domain structures and switching were studied. For example, Chen et al. studied the stability and switching patterns of domain structures in ferroelectric thin films subjected to mechanical loads and related flexoelectric fields (Chen et al. 2015). As shown in Fig. 5a and b, a mixed *a*/*c* domain structure can be switched to a single-domain structure by cylindrical bending with a large surface flexoelectric field. For the upward bending case shown in Fig. 5a, the out-of-plane c^- domains are gradually switched to in-plane at first and then are switched to the out-of-plane c^+, while for the downward bending case shown in Fig. 5b, all in-plane domains are switched to the out-of-plane c^- domain. These two switching patterns can be understood from the different flexoelectric fields due to the different bending directions. For the film with an upward bending, the induced flexoelectric field is upward, leading to the switching of polarization to c^+. For the film with a downward bending, the induced flexoelectric field is downward, leading to the switching of polarization to c^-.

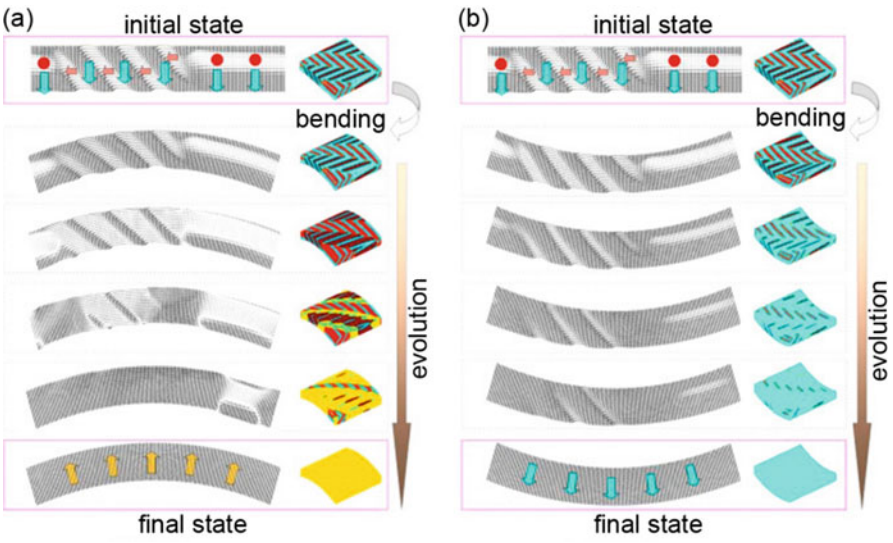

Fig. 5 Switching behavior of the domain structure from *a*/*c* mixed structures to (**a**) single out-of-plane c^+ domain under upward bending and to (**b**) single out-of-plane c^- domain under downward bending. (Adapted from Chen et al. 2015. Copyright 2015, Elsevier)

4 Toward a Multiscale Simulation

Although the thin-film phase-field method has gained great success in understanding the experimental domain structures and phase transitions, and in predicting the domain structures and switching in thin films under conditions beyond the experiment, it has only been applied to limited material systems due to the lack of the thermodynamic parameters including the Landau coefficients, electrostrictive coefficients, elastic constants, and gradient energy coefficients. For example, up to now, there are very limited materials that have available Landau potentials such as $BaTiO_3$, $PbTiO_3$, $PbZr_{1-x}Ti_xO_3$, $BiFeO_3$, $CaTiO_3$, $SrTiO_3$, $KNa_{1-x}Nb_xO_3$, $LiNbO_3$, $LiTaO_3$, $SrBi_2Nb_2O_9$, and $Sr_{0.8}Bi_{2.2}Ta_2O_9$. However, the ferroelectrics that have been discovered are far more beyond these. In order to obtain the Landau coefficients, the polarization and dielectric responses including both the first-order and higher-order dielectric stiffness as function of temperature have to be measured, which is experimentally challenging especially when the required temperature range is broad. An alternative approach to obtaining the Landau coefficients is the first-principle calculation, which has been employed to obtain the Landau coefficients for $BaTiO_3$ (Íñiguez et al. 2001; Geneste 2009), $CaTiO_3$ (Eklund 2010; Gu et al. 2012), and $BiFeO_3$ (Marton et al. 2017). In addition to the Landau coefficients, the first-principle method has also been employed to calculate the phase transitions (Zhong et al. 1994), elastic constants (Wu et al. 2005), electrostrictive coefficients (Wang

et al. 2010), and polarization domain wall energies (Wang et al. 2013; Diéguez et al. 2013; Li et al. 2014). For the domain wall motion speed which is related to the kinetic coefficient L in the TDGL equation, it can be studied using the atomistic molecular dynamics and coarse-grained Monte Carlo simulations (Shin et al. 2007). All these efforts point toward the multiscale simulation-assisted phase-field modeling for ferroelectric thin films (Völker et al. 2011a, 2011b), which can provide principal inputs for future high-throughput calculation (Shen et al. 2017) and optimization of properties and microstructure design for ferroelectric thin films using machine learning (Li et al. 2017).

Acknowledgments The research works on the domain structures and switching in ferroelectric thin films reviewed in this article have primarily been supported by the US Department of Energy, Office of Basic Energy Sciences, Division of Materials Sciences and Engineering under Award DE-FG02-07ER46417, and the works on the strain and flexoelectric effects by the National Science Foundation under DMR-1410714 and by the Penn State MRSEC, Center for Nanoscale Science, under the award NSF DMR-1420620. During the preparation of this manuscript, J. J. Wang also acknowledges the partial support for his effort from the Army Research Office under grant number W911NF-17-1-0462.

References

Ahluwalia R, Tagantsev AK, Yudin P, Setter N, Ng N, Srolovitz DJ (2014) Influence of flexoelectric coupling on domain patterns in ferroelectrics. Phys Rev B 89:174105

Artemev A, Geddes B, Slutsker J, Roytburd A (2008) Thermodynamic analysis and phase field modeling of domain structures in bilayer ferroelectric thin films. J Appl Phys 103:074104

Boettinger WJ, Warren JA, Beckermann C, Karma A (2002) Phase field simulation of solidification. Ann Rev Mater Res 32:163

Bratkovsky AM, Levanyuk AP (2002) Elastic domain structure and the transition between polydomain and monodomain states in thin epitaxial films. Phys Rev B 65:094102

Britson J, Nelson C, Pan XQ, Chen LQ (2014) First-order morphological transition of ferroelastic domains in ferroelectric thin films. Acta Mater 75:188–197

Catalan G, Scott JF (2009) Physics and applications of bismuth ferrite. Adv Mater 21:2463–2485

Chao AY, Arthur AY (1975) Molecular beam epitaxy. Prog Solid State Chem 10:157–192

Chen LQ (2002) Phase-field models for microstructure evolution. Annu Rev Mater Res 32:113

Chen LQ (2008) Phase-field method of phase transitions/domain structures in ferroelectric thin film s: a review. J Am Ceram Soc 91:1835–1844

Chen HT, Soh AK, Ni Y (2014) Phase field modeling of flexoelectric effects in ferroelectric epitaxial thin films. Acta Mech 225:1323–1333

Chen WJ, Zheng Y, Feng X, Wang B (2015) Utilizing mechanical loads and flexoelectricity to induce and control complicated evolution of domain patterns in ferroelectric nanofilms. J Mech Phys Solids 79:108–113

Choi KJ, Biegalski M, Li YL, Sharan A, Schubert J, Uecker R, Reiche P, Chen YB, Pan XQ, Gopalan V, Chen LQ, Schlom DG, Eom CB (2004) Enhancement of ferroelectricity in strained $BaTiO_3$ thin films. Science 306:1005

Choudhury S, Li YL, Chen LQ (2005) A phase diagram for epitaxial $PbZr_{1-x}Ti_xO_3$ thin films at the bulk morphotropic boundary composition. J Am Ceram Soc 88:1669–1672

Cross LE (1996) Ferroelectric materials for electromechanical transducer applications. Mater Chem Phys 43:108–115

Cross LE, Jang SJ, Newnham RE, Nomura S, Uchino K (1980) Large electrostrictive effects in relaxor ferroelectrics. Ferroelectrics 23:187–191

Diéguez O, Aguado-Puente P, Junquera J, Íñiguez J (2013) Domain walls in a perovskite oxide with two primary structural order parameters: first-principles study of $BiFeO_3$. Phys Rev B 89:059901

Eckstein J, Bozovic I (1995) High-temperature superconducting multilayers and heterostructures grown by atomic layer-by-layer molecular beam epitaxy. Annu Rev Mater Sci 25:679–709

Eklund CJ (2010) Ph.D. thesis, Rutgers University, New Brunswick

Emelyanov AY, Pertsev NA, Kholkin AL (2002) Effect of external stress on ferroelectricity in epitaxial thin films. Phys Rev B 66:214108

Frey T, Chi CC, Tsuei CC, Shaw T, Bozso F (1994) Effect of atomic oxygen on the initial growth mode in thin epitaxial cuprate films. Phys Rev B 49:3483–3491

Geneste G (2009) Landau free energy of ferroelectric crystals by thermodynamic integration. Phys Rev B 79:064101

Gránásy L et al (2006) Phase field theory of crystal nucleation and polycrystalline growth: a review. J Mater Res 21:309

Gu YJ, Rabe K, Bousquet E, Gopalan V, Chen LQ (2012) Phenomenological thermodynamic potential for $CaTiO_3$ single crystals. Phys Rev B 85:064117

Gu YJ, Li ML, Morozovska AN, Wang Y, Eliseev EA, Gopalan V, Chen LQ (2014) Flexoelectricity and ferroelectric domain wall structures: phase-field modeling and DFT calculations. Phys Rev B 89:174111

Haeni JH, Irvin P, Chang W, Uecker R, Reiche P, Li YL, Choudhury S, Tian W, Hawley ME, Craigo B, Tagantsev AK, Pan XQ, Streiffer SK, Chen LQ, Kirchoefer SW, Levy J, Schlom DG (2004) Room-temperature ferroelectricity in strained $SrTiO_3$. Nature 430:758

Haun MJ, Furman E, Jang SJ, Cross LE (1989a) Thermodynamic theory of the lead zirconate-titanate solid solution system, part I: phenomenology. Ferroelectrics 99:13–25

Haun MJ, Furman E, McKinstry HA, Cross LE (1989b) Thermodynamic theory of the lead zirconate-titanate solid solution system, part II: Tricritical behavior. Ferroelectrics 99:27–44

Haun MJ, Zhuang ZQ, Furman E, Jang SJ, Cross LE (1989c) Thermodynamic theory of the lead zirconate-titanate solid solution system, part III: curie constant and sixth-order polarization interaction dielectric stiffness coefficients. Ferroelectrics 99:45–54

Hong ZJ, Britson J, Hu JM, Chen LQ (2014) Local 90 degrees switching in $Pb(Zr_{0.2}Ti_{0.8})O_3$ thin film: phase-field modeling. Acta Mater 73:75–82

Hubler GK (1992) Pulsed laser deposition. MRS Bull 17:26–29

Íñiguez J, Ivantchev S, Perez-Mato JM, García A (2001) Devonshire-landau free energy of $BaTiO_3$ from first principles. Phys Rev B 63:144103

Junquera J, Ghosez P (2003) Critical thickness for ferroelectricity in perovskite ultrathin films. Nature 422:506

Karpinsky DV, Eliseev EA, Xue F, Silibin MV, Franz A, Glinchuk MD, Troyanchuk IO, Gavrilov SA, Gopalan V, Chen LQ, Morozovska AN (2017) Thermodynamic potential and phase diagram for multiferroic bismuth ferrite (BiFeO3). npj Comput Mater 3:20

Khachaturyan AG (1983) Theory of structural transformations in solid. Wiley, New York

Kiguchi T, Aoyagi K, Ehara Y, Funakubo H, Yamada T, Usami N, Konno TJ (2011) Configuration and local elastic interaction of ferroelectric domains and misfit dislocation in $PbTiO_3/SrTiO_3$ epitaxial thin films. Sci Technol Adv Mater 12:034413

Kontsos A, Landis CM (2010) Phase-field modeling of domain structure energetics and evolution in ferroelectric thin films. J Appl Mech 77:041014

Koster G, Rijnders GJHM, Blank DHA, Rogalla H (1999) Imposed layer-by-layer growth by pulsed laser interval deposition. Appl Phys Lett 74:3729

Kouhar VG, Pertsev NA, Waser R (2001) Thermodynamic theory of epitaxial ferroelectric thin films with dense domain structures. Phys Rev B 64:214103

Kwo J, Hong M, Trevor DJ, Fleming RM, White AE, Farrow RC, Kortan AR, Short KT (1988) In situ epitaxial growth of $Y_1Ba_2Cu_3O_{7-x}$ films by molecular beam epitaxy with an activated oxygen source. Appl Phys Lett 53:2683

Lee KS, Choi JH, Lee JY, Baik S (2001) Domain formation in epitaxial Pb(Zr,Ti)O3 thin films. J Appl Phys 90:4095

Li ML, Gu YJ, Wang Y, Chen LQ, Duan WH (2014) First-principles study of 180° domain walls in $BaTiO_3$: mixed Bloch-Neel-Ising character. Phys Rev B 90:054106

Li Q, Nelson CT, Hsu SL, Damodaran AR, Li LL, Yadav AK, McCarter M, Martin LW, Ramesh R, Kalinin SV (2017) Quantification of flexoelectricity in $PbTiO_3/SrTiO_3$ superlattice polar vortices using machine learning and phase-field modeling. Nat Commun 8:1468

Li YJ, Wang JJ, Ye JC, Ke XX, Gou GY, Wei Y, Xue F, Wang J, Wang CS, Peng RC, Deng XL, Yang Y, Ren XB, Chen LQ, Nan CW, Zhang JX (2015) Mechanical switching of nanoscale multiferroic phase boundaries. Adv Funct Mater 25:3405–3413

Li YL, Chen LQ (2006) Temperature-strain phase diagram for $BaTiO_3$ thin films. Appl Phys Lett 88:072905

Li YL, Hu SY, Liu ZK, Chen LQ (2001) Phase-field model of domain structures in ferroelectric thin films. Appl Phys Lett 78:3878–3880

Li YL, Hu SY, Liu ZK, Chen LQ (2002a) Effect of substrate constraint on the stability and evolution of ferroelectric domain structures in thin films. Acta Mater 50:395–411

Li YL, Hu SY, Liu ZK, Chen LQ (2002b) Effect of electrical boundary conditions on ferroelectric domain structures in thin films. Appl Phys Lett 81:427–429

Li YL, Choudhury S, Liu ZK, Chen LQ (2003a) Effect of external mechanical constraints on the phase diagram of epitaxial $PbZr_{1-x}Ti_xO_3PbZr_{1-x}Ti_xO_3$ thin films – thermodynamic calculations and phase-field simulations. J Appl Phys 83:1608

Li YL, Hu SY, Chen LQ (2003b) Ferroelectric domain morphologies of (001)$PbZr_{1-x}Ti_xO_3$ epitaxial thin films. J Appl Phys 97:034112

Li YL, Cross LE, Chen LQ (2005) A phenomenological thermodynamic potential for $BaTiO_3$ single crystals. J Appl Phys 98:064101

Li YL, Choudhury S, Haeni JH, Biegalski MD, Vasudevarao A, Sharan A, Ma HZ, Levy J, Gopalan V, Trolier-McKinstry S, Schlom DG, Jia QX, Chen LQ (2006) Phase transitions and domain structures in strained pseudocubic (100) $SrTiO_3$ thin films. Phys Rev B 73: 184112

Li YL, Hu SY, Choudhury S, Baskes MI, Saxena A, Lookman T, Jia QX, Schlom DG, Chen LQ (2008) Influence of interfacial dislocations on hysteresis loops of ferroelectric films. J Appl Phys 104:104110

Liang LY, Li YL, Chen LQ, Hu SY, Lu GH (2009) A thermodynamic free energy function for potassium niobate. Appl Phys Lett 94:072904

Liu GQ, Zhang Q, Huang HH, Munroe P, Nagarajan V, Simons H, Hong ZJ, Chen LQ (2016) Reversible polarization rotation in epitaxial ferroelectric bilayers. Adv Mater Interfaces 3:1600444

Ma H, Chen L, Wang JL, Ma J, Boey F (2008) Strain effects and thickness dependence of ferroelectric properties in epitaxial $BiFeO_3$ thin films. Appl Phys Lett 92:182902

Martin LW, Rappe AM (2017) Thin-film ferroelectric materials and their applications. Nat. Rev. Mater. 2:16087

Marton P, Klíč A, Paściak M, Hlinka J (2017) First-principles-based landau-Devonshire potential for $BiFeO_3$. Phys Rev B 96:174110

Pertsev NA, Zembilgotov AG, Tagantsev AK (1998) Effect of mechanical boundary conditions on phase diagrams of epitaxial ferroelectric thin films. Phys Rev Lett 80:1988

Pertsev NA, Zembilgotov AG, Tagantsev AK (1999) Equilibrium states and phase transitions in epitaxial ferroelectric thin films. Ferroelectrics 223:79–90

Pertsev NA, Kukhar VG, Kohlstedt H, Waser R (2003) Phase diagrams and physical properties of single-domain epitaxial $Pb(Zr_{1-x}Ti_x)O_3$ thin films. Phys Rev B 67:054107

Pohlmann H, Wang JJ, Wang B, Chen LQ (2017) A thermodynamic potential and the temperature-composition phase diagram for single-crystalline $K_{1-x}Na_xNbO_3$ ($0 \leq x \leq 0.5$). Appl Phys Lett 110:102906

Qiu QY, Mahjoub R, Alpay SP, Nagarajan V (2010) Misfit strain-film thickness phase diagrams and related electromechanical properties of epitaxial ultra-thin lead zirconate titanate films. Acta Mater. 58:823–835

Ramesh R, Luther K, Wilkens B, Hart DL, Wang E, Tarascon JM, Inam A, Wu XD, Venkatesan T (1990) Epitaxial growth of ferroelectric bismuth titanate thin films by pulsed laser deposition. Appl Phys Lett 57:1505

Roytburd AL (1998) Thermodynamics of polydomain heterostructures. I. Effect of macrostresses. J. Appl. Phys. 83:228–238

Rupprecht G, Bell RO (1964) Dielectric constant in paraelectric perovskites. Phys Rev 135:A748

Schlom DG, Eckstein JN, Hellman ES, Streiffer SK, Harris JS, Beasley MR, Bravman JC, Geballe TH, Webb C, Dessonneck KE, Turner F (1988) Molecular beam epitaxy of layered Dy–Ba–Cu–O com-pounds. Appl Phys Lett 53:1660

Schlom DG, Chen, LQ, Eom CB, Rabe KM, Streiffer SK, Triscone JM (2007) Strain tuning of ferroelectric thin films. Ann. Rev. Mater. Res. 37:589–626

Schlom DG, Chen LQ, Pan XQ, Schmehl A, Zurbuchen MA (2008) A thin film approach to engineering functionality into oxides. J. Am. Ceram. Soc. 91:2429–2454

Schlom DG, Chen LQ, Fennie CJ, Gopalan V, Muller DA, Pan XQ, Ramesh R, Uecker R (2014) Elastic strain engineering of ferroic oxides. MRS Bulletin 39:118–130

Scott JF (1988) Properties of ceramic KNO_3 thin film memories. Physica B 150:160–167

Scott JF (1991) Phase transitions in ferroelectric thin films. Phase Trans 30:107–110

Seifert A, Lange FF, Speck JS (1995) Epitaxial growth of $PbTiO_3$ thin films on (001) $SrTiO_3$ from solution precursors. J Mater Res 10:680–691

Shen ZH, Wang JJ, Lin YH, Nan CW, Chen LQ, Shen Y (2017) High-throughput phase-field design of high-energy-density polymer nanocomposites. Adv Mater 30:1704380

Sheng G, Hu JM, Zhang JX, Li YL, Choudhury S, Jia QX, Liu ZK, Chen LQ (2008) Misfit strain-misfit strain diagram of epitaxial $BaTiO_3$ thin films: Thermodynamic calculations and phase-field simulations. Appl. Phys. Lett. 93:232904

Shin YH, Grinberg I, Chen IW, Rappe AM (2007) Nucleation and growth mechanism of ferroelectric domain-wall motion. Nature 449:881–884

Shirokov VB, Yuzyuk YI, Dkhil B, Lemanov VV (2007) Phenomenological theory of phase transitions in epitaxial $BaTiO_3$ thin films. Phys Rev B 75:224116

Shirokov VB, Yuzyuk YI, Dkhil B, Lemanov VV (2009) Phenomenological theory of phase transitions in epitaxial $Ba_xSr_{1-x}TiO_3$ thin films. Appl. Phys. Lett. 79:144118

Spah RJ, Hess HF, Stormer HL, White AE, Short KT (1988) Parameters for *in situ* growth of high Tc superconducting thin films using an oxygen plasma source. Appl Phys Lett 53:441

Steinbach I (2009) Phase-field models in materials science. Model Simul Mater Sci Eng 17: 073001

Sundar V, Newnham RE (1992) Electrostriction and polarization. Ferroelectrics 135:431–446

Tagantsev AK (2008) Landau expansion for ferroelectrics: which variable to use? Ferroelectrics 375:19

Tang YL, Zhu YL, Wang YJ, Wang WY, Xu YB, Ren WJ, Zhang ZD, Ma XL (2014) Atomic-scale mapping of dipole frustration at 90^o charged domain walls in ferroelectric $PbTiO_3$ films. Sci Rep 4:4115

Theis CD, Yeh J, Schlom DG, Hawley ME, Brown GW (1998) Adsorption-controlled growth of $PbTiO_3$ by reactive molecular beam epitaxy. Thin Solid Films 325:107–114

Völker B, Marton P, Elsässer C, Kamlah M (2011a) Multiscale modeling for ferroelectric materials: a transition from the atomic level to phase-field modeling. Contin Mech Thermodyn 23: 435–451

Völker B, Landis CM, Kamlah M (2011b) Multiscale modeling for ferroelectric materials: multiscale modeling for ferroelectric materials: identification of the phase-field model's free energy for PZT from atomistic simulations. Smart Mater Struc 21:035025

Wang JJ, Meng FY, Ma XQ, Xu MX, Chen LQ (2010) Lattice, elastic, polarization, and electrostrictive properties of $BaTiO_3$ from first-principles. J Appl Phys 108:034107

Wang JJ, Wang Y, Ihlefeld JF, Hopkins PE, Chen LQ (2016) Tunable thermal conductivity via domain structure engineering in ferroelectric thin films: a phase-field simulation. Acta Mater 111:220–231

Wang Y, Nelson C, Melville A, Winchester B, Shang SL, Liu ZK, Schlom DG, Pan XQ, Chen LQ (2013) $BiFeO_3$ domain wall energies and structures: a combined experimental and density functional theory plus U study. Phys Rev Lett 110:267601

Wang YL, Tagantsev AK, Damjanovic D, Setter N (2007) Landau thermodynamic potential for $BaTiO_3$. J Appl Phys 101:104115

Winchester B, Wu PP, Chen LQ (2011) Phase-field simulation of domain structures in epitaxial $BiFeO_3$ films on vicinal substrates. Appl Phys Lett 99:052903

Wu XF, Vanderbilt D, Hamann DR (2005) Systematic treatment of displacements, strains, and electric fields in density-functional perturbation theory. Phys Rev B 72:035105

Wu PP, Ma XQ, Li YL, Gopalan V, Chen LQ (2012) Dipole spring ferroelectrics in superlattice $SrTiO_3/BaTiO_3$ thin films exhibiting constricted hysteresis loops. Appl Phys Lett 100:092905

Wu PP, Ma XQ, Li YL, Eom CB, Schlom DG, Gopalan V, Chen LQ (2015) Influence of interfacial coherency on ferroelectric switching of superlattice $BaTiO_3/SrTiO_3$. Appl Phys Lett 107:122906

Xu RJ, Zhang JL, Chen ZH, Martin LW (2015) Orientation-dependent structural phase diagrams and dielectric properties of $PbZr_{1-x}Ti_xO_3$ polydomain thin films. Phys Rev B 91:144106

Xue F, Wang JJ, Sheng G, Huang E, Cao Y, Huang HH, Munroe P, Mahjoub R, Li YL, Nagarajan V, Chen LQ (2013) Phase field simulations of ferroelectrics domain structures in $PbZr_xTi_{1-x}O_3$ bilayers. Acta Mater 61:2909–2918

Xue F, Li YJ, Gu YJ, Zhang JX, Chen LQ (2016) Strain phase separation: formation of ferroelastic domain structures. Phys Rev B 94:220101

Xue F, Ji YZ, Chen LQ (2017) Theory of strain phase separation and strain spinodal: applications to ferroelastic and ferroelectric systems. Acta Mater 133:147–159

Yamada T (1972) Electromechanical properties of oxygen-octahedra ferroelectric crystals. J Appl Phys 43:328

Zeches RJ, Rossell MD, Zhang JX, Hatt AJ, He Q, Yang CH, Kumar A, Wang CH, Melville A, Adamo C, Sheng G, Chu YH, Ihlefeld JF, Erni R, Ederer C, Gopalan V, Chen LQ, Schlom DG, Spaldin NA, Martin LW, Ramesh R (2009) A strain-driven morphotropic phase boundary in $BiFeO_3$. Science 326:977–980

Zembilgotov AG, Pertsev NA, Böttger U, Waser R (2005) Effect of anisotropic in-plane strains on phase states and dielectric properties of epitaxial ferroelectric thin films. Appl Phys Lett 86:052903

Zhang JX, Li YL, Wang Y, Liu ZK, Chen LQ, Chu YH, Zavaliche F, Ramesh R (2007) Effect of substrate-induced strains on the spontaneous polarization of epitaxial $BiFeO_3$ thin films. J Appl Phys 101:114105

Zhang JX, Li YL, Choudhury S, Chen LQ, Chu YH, Zavaliche F, Cruz MP, Ramesh R, Jia QX (2008) Computer simulation of ferroelectric domain structures in epitaxial $BiFeO_3$ thin films. J Appl Phys 103:094111

Zhang W, Ouyang J, Roytburd AL (2012) Effect of thickness-mediated misfit strain on the heterophase polydomain structure of epitaxial $BiFeO_3$ films. Script Mater 66:499–502

Zhong WL, Vanderbilt D, Rabe KM (1994) Phase transitions in $BaTiO_3$ from first principles. Phys Rev Lett 73:1861